1 **Emission Factors and Optical Properties of Black and Brown Carbon Emitted at a Mixed-**

2 **Conifer Forest Prescribed Burn**

4 James D.A. Butler,[1,2] Afsara Tasnia,[3] Deep Sengupta,[4] Nathan Kreisberg,[5] Kelley C. Barsanti,[3,6]

5 Allen H. Goldstein,[1,5] Chelsea V. Preble,[1,2] Rebecca A. Sugrue,[1,2] Thomas W. Kirchstetter[1,2,*]

7 [1]Department of Civil and Environmental Engineering, University of California, Berkeley,

8 Berkeley, California 94720

10 [2]Energy Technologies Area, Lawrence Berkeley National Laboratory, Berkeley, California 94720

12 [3]Department of Chemical and Environmental Engineering, Center for Environmental Research

13 and Technology, University of California, Riverside, Riverside, California 92507

15 [4]Department of Environmental Science, Policy, and Management, University of California,

16 Berkeley, Berkeley, California 94720

18 [5]Aerosol Dynamics Inc., Berkeley, California 94720

20 [6] Atmospheric Chemistry Observations and Modeling, U.S. National Science Foundation

21 National Center for Atmospheric Research, Boulder, Colorado 80301

23 *Corresponding author email: twkirchstetter@lbl.gov

Abstract

Prescribed burning is a fuel management practice employed globally that emits carbonaceous aerosols that affect human health and perturb the global climate system. Fuel-based black and brown carbon (BC and BrC) emission factors were calculated from ground and aloft smoke during prescribed burns at a mixed-conifer, montane forest site in the Sierra Nevada in California. BC emission factors were 0.52 ± 0.42 and 1.0 ± 0.48 g kg^{-1} for the smoldering and flaming combustion phases. Modified combustion efficiency is a poor predictor of BC emission factor, in this study and published literature. We discuss limitations of using generalized BC to PM$_{2.5}$ mass emission ratios to generate emission inventories; using BC emission factors measured in this study, we recommend BC to PM$_{2.5}$ ratios of 0.7% and 9.5% for the smoldering and flaming combustion in mixed conifer prescribed burns. We apportioned the measured aerosol spectral absorption between BrC and BC and calculated absorption Ångström exponents (AAE) of 6.26 and 0.67, respectively. Using a BrC-specific absorption cross-section, we estimated BC concentrations and a smoldering combustion BrC emission factor of 7.0 ± 2.7 g kg^{-1}, nearly 14 and 7 times greater than the smoldering and flaming BC emission factors. Furthermore, we estimate that BrC would account for 23% and 82%, respectively, of the solar radiation absorbed by the smoldering smoke in the atmosphere integrated over the solar spectrum (300–2500 nm) and in the UV spectrum (300–400 nm), indicating that BrC affects tropospheric photochemistry in addition to atmospheric warming.

Key Figure
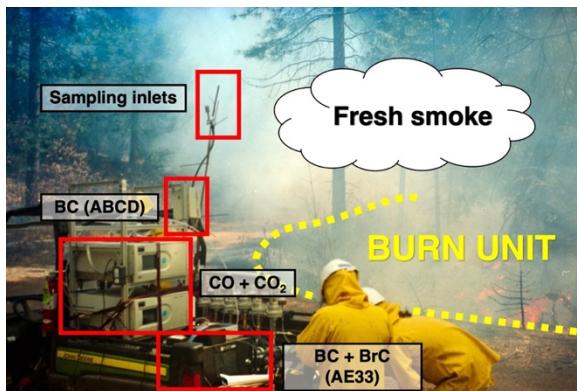
Keywords

Prescribed burn, black carbon, brown carbon, emission factor, light absorbing aerosol, wildland fire fuel consumption model

1 Introduction

Prescribed burns are controlled burns that consume excess and dead fuel in an ecosystem, like the duff, shrubs and dead biomass in the forest understory, or floor. In contrast, wildfires are uncontrolled burns that may consume both the understory and overstory, or canopy, of a forest and may spread to nearby property, endangering the homes and lives of people in the wildland urban interface. Routine prescribed burns, or other fuel management practices like mechanical thinning, reduce the risk and severity of wildfire ignition in forest ecosystems and increase the resistance to ecosystem transition (i.e., conversion of forest to shrubland) caused by wildfires (Steel et al., 2021; Wu et al., 2023).

Prescribed burns and wildfires emit fine particulate matter ($PM_{2.5}$), carbon monoxide (CO), carbon dioxide (CO_2), volatile organic compounds, and nitrogen oxides (Andreae, 2019; Urbanski, 2014; Urbanski et al., 2008; Wiedinmyer et al., 2006). Emitted $PM_{2.5}$ includes organic aerosol, some of which is light-absorbing brown carbon (BrC), and black carbon (BC). Whereas BC absorbs solar radiation broadly across the visible spectrum, BrC light absorption is highly wavelength dependent and strongest in the near-UV spectral region (Bond et al., 2004; Kirchstetter et al., 2004; Laskin et al., 2015). Due to their perturbation of the radiative balance of the atmosphere and short atmospheric residence time compared to CO_2, BC, and BrC are considered short-lived climate forcers (Feng et al., 2013; Kirchstetter and Thatcher, 2012; Zhang et al., 2020). Additionally, BC and BrC surface deposition in snowy climates reduces the solar reflectance of snow and may accelerate snow melt (Chelluboyina et al., 2024; Hadley and Kirchstetter, 2012; Kaspari et al., 2015; Yang et al., 2015). Human exposure to carbonaceous aerosols also has detrimental health effects including cardiovascular disease, lung cancer, adverse birth outcomes, and premature mortality (Dong et al., 2023; Grahame et al., 2014; Janssen et al., 2011). Wildland fires are a major source of pollution relevant to human exposure and account for one third of total $PM_{2.5}$ emissions in the U.S., with roughly equal contributions from prescribed burns and wildfires (Larkin et al., 2020).

77   Wildland fire modeling frameworks, or smoke models, estimate the amount of smoke

78   emitted during burn events to create input emissions necessary for climate modeling, air

79   pollution modeling, and health impact assessments (California Air Resources Board, 2020;

80   Connolly et al., 2024; Cruz Núñez et al., 2014; Maji et al., 2024). Smoke emissions from

81   wildland fires are estimated with fuel consumption models like Burnup, part of the First-Order

82   Fire Effects Model (FOFEM), and CONSUME, part of the BlueSky Smoke Modeling

83   Framework (Keane and Lutes, 2018; BlueSky Modeling Framework, 2024). Both smoke models

84   compute total emissions of a pollutant by multiplying pollutant emission factors by the mass of

85   fuel consumed during both the high intensity and low intensity stages of a burn event, which

86   roughly correspond to the flaming and smoldering phases of a wildland fire.

87   The differences in fuel mass consumption and temperature in these phases affect the

88   emission rate of pollutants, sometimes by an order of magnitude. In the flaming phase, fuel mass

89   consumption and temperature are highest and combustion is more complete, while both are lower

90   in the smoldering phase that is characterized by incomplete combustion (Urbanski, 2014).

91   Flaming combustion generally has a higher emission rate of BC and a lower emission rate of BrC

92   compared with smoldering combustion, while smoldering combustion is marked by higher

93   emissions of CO and BrC (Chen et al., 2007). Experiments designed to quantify pollutant

94   emissions must consider the placement of sampling instrumentation to capture these distinct

95   combustion phases of a burn, with aerial sampling platforms more likely to capture a mixture of

96   flaming and smoldering combustion due to the convective lofting of smoke caused by flaming

97   combustion (Aurell et al., 2021). Ground-level smoke, on the other hand, tends to be dominated

98   from smoldering combustion (Aurell and Gullett, 2013).

99   In this study, we conducted field sampling of pollutant emissions from prescribed burning

100   of a mixed-conifer understory and computed BC emission factors, BrC emission factors, and

101   aerosol absorption properties with ground and aerial sampling platforms. We investigate the

102   relationship between BC emission factors and combustion conditions and, finding that the

103   modified combustion efficiency (MCE) is a poor predictor of BC emission factor, propose a

104   framework to aggregate emission factors by either flaming or smoldering conditions to convey

105   the average value and variability of emission factors within these combustion regimes in fuel

106   consumption models. We report BC/$PM_{2.5}$ ratios, or speciation profiles, for a mixed-conifer

107 understory prescribed burn. We then discuss how applying an incorrect $BC/PM_{2.5}$ ratio in

108 wildland fire modeling frameworks may lead to large errors in BC emissions, using the

109 ecosystem studied in this work as an example. We compute the absorption Ångström exponent

110 (AAE) for the prescribed burn smoke aerosols, demonstrating that AAE is sensitive to the

111 wavelengths used in its calculation, and present estimates of AAE separately for BC and BrC to

112 estimate their contributions the solar radiation absorbed by the smoldering smoke in the

113 atmosphere.

114

2 Materials and Methods

2.1 Field Measurements

117   Field measurements were made at the Blodgett Forest Research Station (38.915224, -

118 120.662420), located 1370 meters above sea level on the western slope of the Sierra Nevada, 21

119 km east of Georgetown, CA. Prescribed burns were conducted in a mixed conifer forest, typical

120 of montane ecosystems of the Sierra Nevada (North et al., 2016). Three forest units were burned

121 in consecutive days in April 2021, as shown in Figure S1 in the Supporting Information (SI). The

122 prescribed burn on the first day escaped the designated unit (A) and the burn was terminated

123 early. The remainder of unit A was burned on the second day and units B and C were burned on

124 the third and fourth days, respectively.

125   Prescribed burn smoke was measured using both a ground and an aerial sampling

126 platform. The ground platform consisted of pollutant analyzers secured to a utility task vehicle

127 stationed immediately downwind of the fire to capture fresh smoke two meters above ground

128 level (see Figure S2). The ground platform was moved once each day as the burns progressed

129 and winds shifted to be on service roads nearby the highest intensity burn activity and the aerial

130 platform takeoff/landing location. Across the four days, there were nine ground sampling

131 sessions: at two locations on each day, plus one "next-day" smoldering sample on the second day

132 for burn unit A before ignition of the remaining unit. For the aerial platform, pollutant analyzers

133 were attached to the unmanned aerial vehicle, a DJI Matrice 600 Pro hexacopter. Concurrent

134 with ground sampling, the unmanned aerial vehicle was flown 23 times across the four days with

135 at least five flights each day and a maximum of 10 flights on the third day. The aerial platform

136 was flown in the densest smoke plumes to intercept the bulk of the prescribed burn smoke and

137   hovered within these plumes to capture fresh emissions representative of the event. The average

138   elevation of aerial platform throughout sampling was 29 meters, with an average sampling

139   elevation range of 16–42 meters across all flights.

140   BC, CO, and CO_2 were measured on both the ground and aerial sampling platforms. BC

141   was measured using two filter-based aerosol absorption photometers: the Aerosol Magee

142   Scientific aethalometer model AE33 with a 2.5 μm cyclone on the inlet on the ground platform

143   and the custom-built Aerosol Black Carbon Detector (ABCD) on both the ground and aerial

144   platforms (Caubel et al., 2018; Sugrue et al., 2024). These instruments estimate BC

145   concentrations from measured aerosol light absorption and wavelength-specific absorption cross

146   section. The ABCD estimates BC concentration based on aerosol optical attenuation at 880 nm

147   wavelength (λ). The AE33 also measures BC at λ=880 nm, in addition to aerosol optical

148   attenuation at six other wavelengths. In particular, the AE33 reports the mass concentration UV-

149   absorbing aerosol (UVPM) based on the optical attenuation at 370 nm. BrC concentration was

150   estimated from these data as described below in Section 2.2. Filter-based aerosol absorption

151   photometry has well known limitations due to the interactions of the collected aerosol particles

152   and filter media. Corrections for these sampling artifacts are detailed in the Supporting

153   Information, SI.

154   Collocating the AE33 with the ABCD on the ground enabled an analysis to express BC

155   measured with the ABCD in terms of AE33 equivalence, also described below. CO and CO_2

156   were measured by non-dispersive infrared (NDIR) absorption photometry on the ground

157   platform using Horiba models APMA370 and APCA370, respectively.(Tasnia et al., 2025) CO

158   and CO_2 were measured on the aerial platform with an electrochemical cell (Alphasense CO-B4)

159   and NDIR sensor (PP Systems SBA-5), respectively. All instruments reported pollutant

160   concentrations at 1 Hz frequency. Data were post-processed and validated prior to analysis using

161   the quality assurance and control measures described in the SI, including pollutant concentration

162   time-series alignment and loading artifact correction of BC concentrations measured with the

163   ABCD.

164

165   **2.2 Calculations**

166   Light absorption by carbonaceous aerosols increases with decreasing wavelength, a trend

167   that is often modeled as a power-law:

168    $$b_{abs}(\lambda) \propto \lambda^{-\text{AAE}} \qquad \text{(Equation 1)}$$

169   AAE was calculated by an ordinary least squares linear regression of the natural log

170   transformation of λ and $b_{abs}(\lambda)$. Here, $b_{abs}(\lambda)$ (m^{-1}) was calculated by multiplying the

171   wavelength-dependent, loading artifact-corrected, light-absorbing aerosol concentration reported

172   by the AE33 by the wavelength-dependent mass absorption cross-section of BC on a filter (m^2

173   g^{-1}). Aerosol absorption was calculated per second and then averaged per minute with a 90% data

174   completeness threshold applied at seven wavelengths measured by the ground aethalometer.

175   The Delta-C method has been used to estimate BrC concentrations with a multi-

176   wavelength aethalometer (Harrison et al., 2013; Huang et al., 2011; Stampfer et al., 2020;

177   Wagstaff et al., 2022; Wang et al., 2010, 2011a, b), where BrC is the difference between UVPM

178   and BC concentrations in units of μg m^{-3}:

179    $$BrC = UVPM - BC \qquad \text{(Equation 2)}$$

180   The AE33 aethalometer assumes light absorption at 880 nm is entirely due to BC and UVPM is

181   the mass concentration of all light absorbing aerosol at 370 nm. The AE33 further assumes that

182   UVPM has the same absorption cross-section as BC (i.e., 18.47 m2 g-1 at 370 nm). Thus, a

183   direct application of Equation 2 implicitly assumes that BrC has the same absorption cross-

184   section as BC.

185   In this study, we improve upon this method to estimate BrC concentrations. We first

186   determine the contribution of BrC to total aerosol absorption at 370nm:

187    $$b_{abs,BrC}(370nm) = b_{abs}(370nm) - b_{abs,BC}(370nm) \qquad \text{(Equation 3)}$$

188   We estimate BC absorption at 370 nm, $b_{abs,BC}$(370nm), by extrapolating the measured aerosol

189   light absorption at 880 assuming AAE$_{BC}$ = 0.67. Whereas AAE$_{BC}$ = 1 is a commonly used value

190   that is consistent with Mie theory (i.e., uncoated, ideal spherical particles with wavelength-

191   independent refractive index) (Liu et al., 2018), the value 0.67 was estimated based on the

192   optical properties of the smoke measured in this study, as described below in Section 3.3. We

193   then calculate BrC concentration by dividing $b_{abs,BrC}$(370nm) by the current best estimate of the

194   BrC mass absorption cross-section empirically determined by Ivančič et al. (4.5 m^2 g^{-1} at 370

195   nm) rather than assuming BrC and BC have the same absorption cross-section. In doing so, our

196   BrC concentrations are equivalent to those reported by the newest model of the aethalometer

197   (i.e., the AE36) (Aerosol d.o.o., 2024).

198   Following the approach presented in Kirchstetter and Thatcher (2012), we computed the

199   contribution of BrC to smoldering smoke aerosol absorption of solar radiation. The contribution

200   of BrC to spectral absorption in each smoke sample, $b_{abs,BrC}(\lambda)$, is determined by subtracting the

201   BC absorption from the total absorption with Equation 3. Based on the apportionment of spectral

202   absorption to BC and BrC, we compute the fraction of spectral radiation for smoldering smoke

203   at each wavelength in the solar spectrum that would be absorbed by BrC:

204
$$f_{BrC} = \frac{b_{abs,BrC}(\lambda)}{b_{abs}(\lambda)}$$
(Equation 4)

205   Last, we compute the fraction of solar radiation that BrC in the smoldering smoke would absorb

206   in the atmosphere:

207
$$F_{Brc} = \frac{\int_{\lambda_1}^{\lambda_2} f_{BrC}(\lambda) \cdot i(\lambda) d\lambda}{\int_{\lambda_1}^{\lambda_2} i(\lambda) d\lambda}$$
(Equation 5)

208   where $i(\lambda)$ is the clear sky air mass one global horizontal solar spectrum at the earth's surface

209   (Levinson et al., 2010). We evaluate F_{BrC} using two sets of integration bounds (λ_1, λ_2): (1) across

210   the full solar irradiance spectrum from 300 to 2500 nm that is meaningful for atmospheric

211   warming and (2) in the near-UV from 300 to 400 nm that is more relevant to tropospheric

212   photochemistry (Li and Li, 2023; Mok et al., 2016).

213   The modified combustion efficiency (MCE) is typically used to assess the combustion

214   completeness during biomass burning and was calculated as the mass fraction of fuel C emitted

215   as CO_2 compared to CO_2 and CO (Ward and Radke, 1993):

216
$$MCE = \frac{\Delta CO_2}{\Delta CO_2 + \Delta CO}$$
(Equation 6)

217   Background-subtracted concentrations ΔCO and ΔCO_2 were calculated as the difference between

218   measured concentrations and background concentrations, the latter of which were established

219   separately for each of the four days of sampling (listed in Table S2). MCE is unitless, and a value

220   of 0.9 is commonly used as a threshold to distinguish between flaming-dominated (MCE > 0.9)

221   and smoldering-dominated (MCE < 0.9) combustion (Selimovic et al., 2018).

222   Fuel-based BC and BrC emission factors (EF_i) in units of grams BC and BrC emitted per

223   kilogram fuel consumed (g kg^{-1}) were calculated by the carbon balance method:

$$224 \qquad EF_i = \frac{w_c * V_m}{MW_C} \int_{t_0}^{t_1} \frac{\Delta C_i}{(\Delta CO + \Delta CO_2)} dt \qquad \text{(Equation 7)}$$

225 where ΔC_i is the background-subtracted BC or BrC concentration (μg m^{-3}), $w_c = 0.5$ is the weight

226 fraction of carbon in conifer forest fuels (Thomas and Martin, 2012), V_m is the molar volume of

227 air and equal to 0.024 m^3 mol^{-1}, MW_c is the molar mass of carbon and equal to 12 g mol^{-1}, and

228 ΔCO and ΔCO_2 are mixing ratios (ppm) (Akagi et al., 2011). In Equation (7), the carbon balance

229 method assumes that all fuel carbon is emitted as either CO or CO_2, given 90–98% of total

230 emitted carbon is emitted as these gases (Akagi et al., 2011; Binte Shahid et al., 2024; Nelson Jr.,

231 1982; Yokelson et al., 2013). Emission factors were calculated by integration of the background-

232 subtracted pollutant concentrations over different time intervals. The integration bounds for the

233 aerial emission factors were the start and end times of each flight, with a temporal basis equal to

234 the total flight duration, or $t_1 - t_0$ in Eq. 4. Flight durations ranged from 4–22 minutes. For the

235 ground emission factors, the start time (t_0) was when the aethalometer began collecting samples

236 on a new filter spot and the attenuation (ATN) was zero. The end time (t_1) was when the filter

237 became saturated at an ATN of 100. At that point, the aethalometer advanced its filter tape. These

238 integration bounds resulted in a ground sample temporal basis that corresponded to the ATN

239 cycle of the aethalometer, which ranged from 2–36 minutes. A detailed discussion of the

240 representativeness and chosen temporal basis of the emission factors is provided in the SI.

241

242 **3 Results and Discussion**

243 **3.1 Emission Factors**

244   BC and BrC emission factors measured on the ground and aloft are presented in Table 1.

245 Overall, the aerial platform measured smoke characterized by a higher modified combustion

246 efficiency (MCE$_{aerial}$ = 0.88 ± 0.05, average ± standard deviation) and nearly 2 times higher BC

247 emission factor (EF$_{BC,aerial}$ = 0.92 ± 0.48 g kg^{-1}) than the smoke measured on the ground

248 (MCE$_{ground}$ = 0.83 ± 0.03; EF$_{BC,ground}$ = 0.47 ± 0.40 g kg^{-1}).

249

250 Table 1: Summary Statistics of Carbonaceous Aerosol Emission Factors and MCE (average ±

251 standard deviation)

	Number of Samples	MCE	BC (g kg^{-1})	BrC (g kg^{-1})

Aerial samples	23	0.88 ± 0.05	0.92 ± 0.48	–
Ground samples	66	0.83 ± 0.03	0.47 ± 0.40	7.0 ± 2.7
Smoldering samples	77	<0.9	0.52 ± 0.42	–
Flaming samples	12	>0.9	1.0 ± 0.48	–
All samples	89	0.84 ± 0.04	0.59 ± 0.68	–

252

253   BC emission factors are plotted against MCE in Figure 1. Individual ground platform
254   samples are plotted as orange circles and aerial samples are plotted as blue squares. Nearly all
255   the smoke samples collected from the ground platform (64 of 66 ATN cycles) were associated
256   with smoldering combustion (MCE < 0.9). A roughly equal number smoke samples collected
257   aloft were associated with flaming-dominant combustion (10 flights) and smoldering-dominant
258   combustion (13 flights). BC emission factors demonstrated a weak positive linear correlation
259   (solid black line, $r^2 = 0.11$) against MCE values, with BC emission factors spanning an order of
260   magnitude (0.11 to 1.70 g kg^{-1}) and MCE values ranging from 0.76 to 0.96. This relationship is
261   similar to the weak positive linear trend reported by McMeeking et al. (2009) for a laboratory
262   study ($r^2 = 0.09$), shown as a dashed black line in Figure 1. In contrast, another laboratory study
263   by Hosseini et al. (2013) reported a weak negative linear trend (dotted black line, $r^2 = 0.10$). The
264   application of linear regression models to emission factor data would allow these field and
265   laboratory studies to be scaled in fuel consumption models as a function of combustion
266   conditions and/or fire intensity (Burling et al., 2011; May et al., 2014; Ottmar, 2014; Selimovic
267   et al., 2018; Urbanski, 2014). However, given the very low coefficients of determination from
268   this work and previous laboratory studies ($r^2 < 0.15$), MCE is not a strong predictor of the BC
269   emission factor for smoke model estimates.
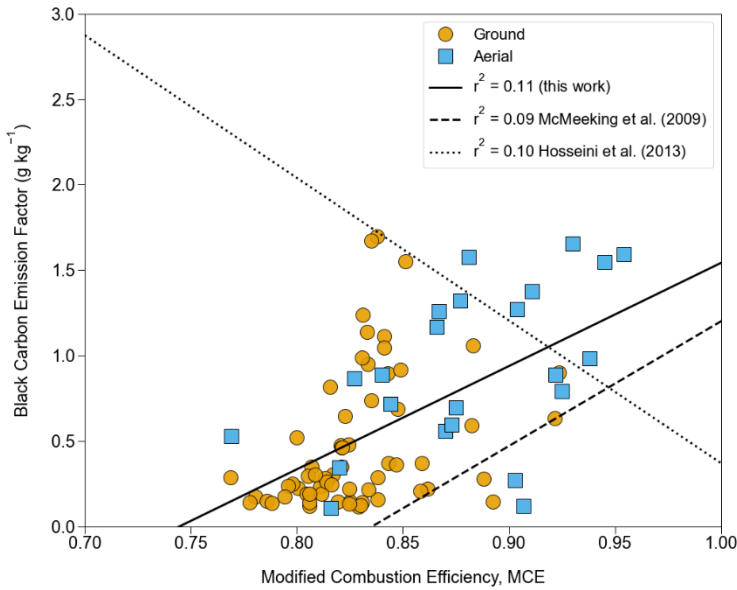
270

271 Figure 1: BC emission factors plotted against modified combustion efficiency for all samples.
272 Symbology designates the ground (circles) and aerial (squares) measurement platforms. All
273 samples fit with a linear regression model and compared to previous laboratory linear models of
274 BC emission factors as a function of MCE (Hosseini et al., 2013; McMeeking et al., 2009).

275

3.2 Emissions Modeling in Fuel Consumption Models

277 BC emission factor distributions for flaming (MCE>0.9) and smoldering (MCE<0.9)

278 conditions are presented in Figure 2. These combustion categories were chosen to match how

279 smoke models calculate emissions, often with combustion-phase dependent emission factors.

280 Fuel consumption models (e.g., Burnup, CONSUME) compute the total fuel consumed

281 separately during flaming and smoldering combustion phases of a burn. Smoke models then

282 apply the appropriate EFs, with either one EF for flaming combustion and one EF for smoldering

283 combustion (e.g., FOFEM), or using a linear model like that presented in Figure 1 where the

284 calculated MCE in the fuel consumption model is used to obtain the corresponding EF. The

285 average BC emission factors measured during flaming combustion conditions in this study were

286 nearly 2 times greater than those measured during smoldering conditions: $EF_{BC,flaming} = 1.0 \pm$

287 0.48 g kg^{-1} versus $EF_{BC, smoldering} = 0.52 \pm 0.42$, with similar magnitude as the average emissions

288 factors for aerial and ground samples reported above.

289
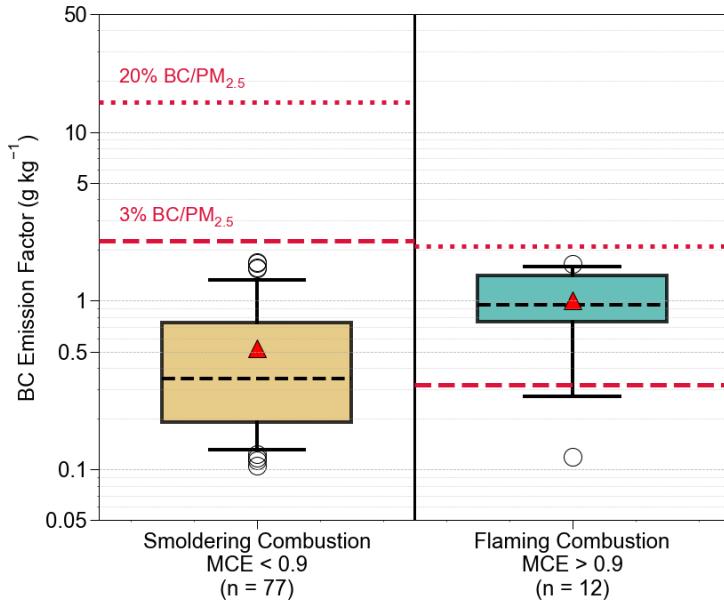
290

291 Figure 2: BC emission factors categorized into smoldering combustion (MCE < 0.9) and flaming
292 combustion (MCE > 0.9) phases for input into fuel consumption. Boxes represent the
293 interquartile range and tails the 5th and 95th percentile. The median is provided as the black
294 dashed line across the box, the average as a red triangle, and outliers as open circles. Speciation
295 profile-derived BC emission factors for 3% and 20% BC/PM$_{2.5}$ for each combustion phase are
296 plotted as red horizontal dashed and dotted lines, respectively. Note the logarithmic scale on the
297 y-axis.

298

299   Also included in Figure 2 are BC emission factors calculated with the FOFEM
300 methodology as a fraction of PM$_{2.5}$ emission factors from Burling et al. (2011) for a mixed-
301 conifer understory prescribed burn (Burling et al., 2011; Lutes, 2020). These BC emission factors
302 are plotted as horizontal lines across each combustion regime in Figure 2 and represent values
303 assumed in the most recent federal and California BC inventories. The 2020 National Emissions
304 Inventory (dashed line) assumes a 3% BC/PM$_{2.5}$ mass ratio for all wildland fire sources,
305 including prescribed burns and wildfires (US Environmental Protection Agency, 2023). The 2013
306 California BC Emissions Inventory (dotted line) assumes a 20% BC/PM$_{2.5}$ mass ratio for
307 prescribed burns (California Air Resources Board, 2016). These BC/PM$_{2.5}$ mass ratios—or BC
308 speciation profiles—are known to be highly uncertain (Chow et al., 2011). For example, in the
309 EPA SPECIATE v5.3 database, prescribed burn BC/PM$_{2.5}$ mass ratios vary from 3–11% and for
310 uncontrolled forest fire or forest fuel types between 0.8–80% (SPECIATE, 2025).

311   The difference between the average flaming and smoldering BC emission factors
312 measured in this study and the BC emission factors estimated from BC/$PM_{2.5}$ ratios reveals the
313 current limitation in using the latter methodology in wildland fire modeling frameworks to
314 estimate BC emissions. $PM_{2.5}$ emission rates for mixed-conifer forests and many other
315 ecosystems are higher under smoldering combustion than under flaming combustion, the
316 opposite of BC emission rates (Burling et al., 2011; Chen et al., 2007). As a result, BC emission
317 rates are erroneously predicted to be greater under smoldering combustion. The speciation
318 profiles assumed in the federal and California inventories overestimate BC emission factors
319 under smoldering combustion for this type of burn by a factor 4 and 29, respectively. Under
320 flaming combustion, the California inventory overestimates BC emission rates by a factor of 2,
321 whereas the federal inventory underestimates by 0.3. Dividing the average field BC emission
322 factors in this study by the $PM_{2.5}$ emission factor from Burling et al. (2011) indicates that a more
323 appropriate BC speciation profile for a mixed-conifer understory prescribed burn would be 0.7%
324 and 9.5% for the smoldering and flaming combustion phases, respectively.
325
326 **3.3 Optical Properties and Apportionment of Aerosol Solar Radiation Absorption**
327   BrC emission factors were computed based on ground-level smoke measurements with
328 the multiwavelength aethalometer, most of which (64 of 66 samples) were during smoldering-
329 dominated combustion. There as a very weak positive linear relationship ($r^2 = 0.06$) between BrC
330 emission factors and MCE (Figure 3). The study average BrC emission factor was 7.0 ± 2.7 g
331 kg^{-1}. It is worth noting that this BrC emission factor, computed as described in Section 2.2 based
332 on an absorption cross-section specific to BrC, is 4.4 times greater than the emission factor
333 calculated using the more traditional Delta-C method, where the absorption-cross section of BrC
334 is operationally defined as equal to the absorption cross-section of BC.
335
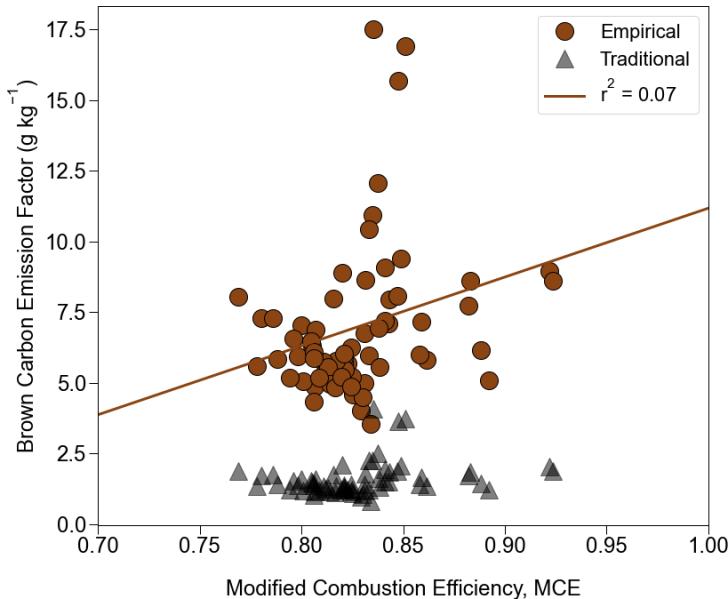
336

337 Figure 3: Ground BrC emission factors computed using the Delta-C method with a BrC-specific
338 mass absorption cross-section (denoted as Empirical and shown with brown circles) and the
339 more traditional approach using an operationally defined BrC mass absorption cross-section
340 equal to that of BC (denoted as Traditional and shown with grey triangles) plotted against
341 modified combustion efficiency. The solid brown line shows the linear regression for the BrC
342 emission factors calculated with the empirical approach.

343

344   Study-average spectral absorption curves are plotted in Figure 4. A power-law fit to the

345 data over all aethalometer wavelengths from 370–950 nm is shown in Figure 4a. The absorption

346 data are fit with two trend lines in Figure 4b: an extrapolation of the power law fit to the near-IR

347 data at 880 and 950 nm to illustrate the BC contribution to total absorption, $b_{abs,BC}(\lambda)$, and a

348 power law fit of the BrC contribution to absorption, $b_{abs,BrC}(\lambda)$, which extends from mid-visible

349 wavelengths to the near-UV, calculated using Eq. 3. The AAE given by the power law exponent

350 reported in Figure 4a is 2.32 (1.35, 3.29; 95% confidence interval), indicating a significant

351 contribution of BrC to total absorption. The power law fits in Figure 4b yield $AAE_{BrC} = 6.26$

352 (5.37, 7.13) and $AAE_{BC} = 0.67$. For comparison, El Asmar et al. (2024) found similar overall

353 AAE = 1.89 (range of 1.31–3.32) and a lower average $AAE_{BrC} = 5.00$ (range of 3.19–7.43) for

354 prescribed burns in southeastern US measured 0–8 hours downwind with the same model

355 multiwavelength aethalometer used in this study. The AAE_{BrC} for western wildfires measured

356 with a photoacoustic spectrometer by Zeng et al. (2022) was also comparable (2.07 ± 1.01;

357 average ± standard deviation). Mie theory predicts that $AAE_{BC} = 1$ for particle diameters less

358 than 10 nm and $AAE_{BC} < 1$ for particle diameters greater than ~0.2 μm (Wang et al., 2016),

359 suggesting that the bulk of sampled aerosols had a diameter greater than 0.2 μm and less than 2.5

360 μm, since a $PM_{2.5}$ cyclone was placed on the sampling inlet.

361
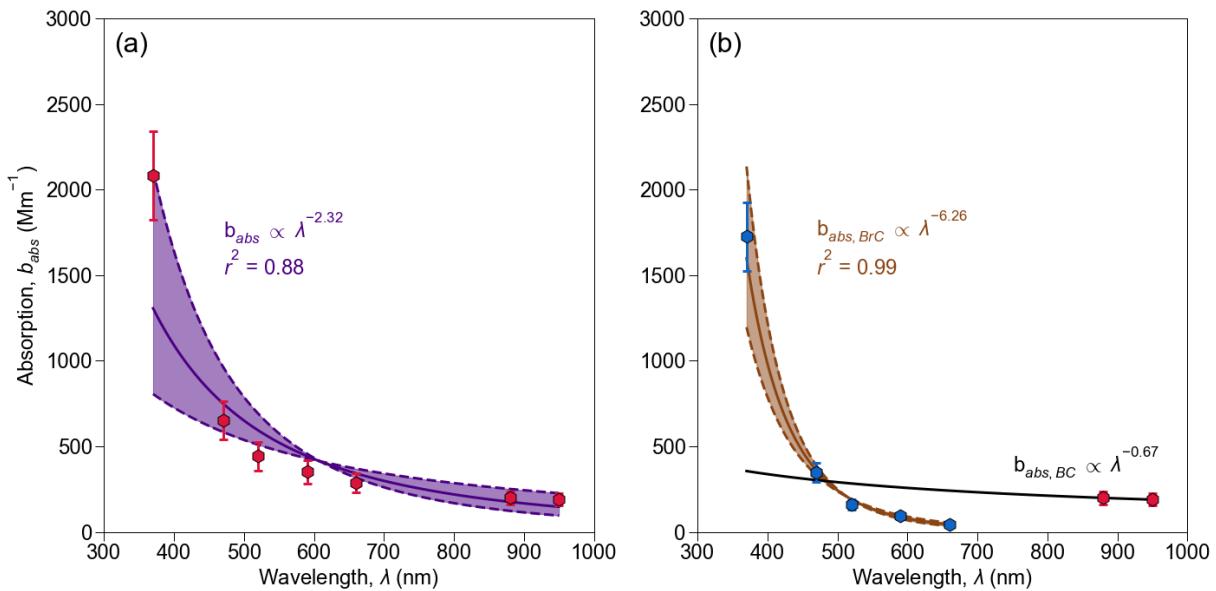
362
363 Figure 4: Average 1-minute absorption at seven wavelengths measured by the ground
364 aethalometer plotted as red hexagons, with error bars representing 95% confidence intervals. (a)
365 Power-law fit of the average absorption curve at all wavelengths with an AAE = 2.32 (solid
366 curve) and 95% confidence interval AAE values displayed as the bounding dashed curves. (b)
367 Power-law fit of the BrC average absorption curve (λ = 370, 470, 520, 590, and 660 nm; blue
368 circles) with an $AAE_{BrC} = 6.26$ (solid brown curve) with 95% confidence interval AAE values
369 displayed as the bounding dashed curves and the BC average absorptions (λ = 880, 950 nm; red
370 hexagons) with an $AAE_{BC} = 0.67$ (solid black curve).

371

372   Whereas the absorption cross-section of BrC is much lower than that of BC over the near-
373 IR to near-UV portion of the solar spectrum, smoldering smoke emits much more BrC than BC:
374 7.0 ± 2.7 gBrC kg^{-1} versus 0.52 ± 0.42 gBC kg^{-1}. Consequently, using Equation 5 and shown in
375 Figure S10, we estimate that BrC and BC would account for 23% and 77% of incoming solar
376 radiation absorbed by the smoldering smoke in the atmosphere (integrated from 300 to 2500
377 nm). Furthermore, BrC would contribute 82% of the aerosol absorption of solar radiation at

378 wavelengths below 400 nm and, therefore, may affect tropospheric photochemistry. Similarly,
379 Chakrabarty et al. (2023) found BrC contributes 66–86% of total aerosol absorption at 405 nm in
380 wildfire smoke emitted in the western United States.
381   AAE values reported in the literature are computed using different approaches. For
382 example, AAE is commonly derived from data at only two wavelengths and those wavelengths
383 differ from study to study, which makes direct comparison among studies challenging. To
384 illustrate this point, we calculated AAE values on 1-minute absorption data from the current
385 study using three wavelength pairs that approximate prior work. Table 2 reports power law fitting
386 of (i) 370 and 880 nm to approximate the wavelengths in a photoacoustic extinctiometer, (ii) 470
387 and 660 nm to approximate a continuous light absorption photometer, and (iii) 470 and 880 nm
388 to approximate the satellite based AERONET.
389
390 Table 2: Measured and Nearest Aethalometer Wavelengths to Calculate the Absorption Ångström
391 Exponent (AAE)

Carbonaceous Aerosol Measurement Method	Example Studies	Measured Wavelengths, λ (nm)	Nearest Aethalometer Wavelengths, λ (nm)	AAE, Average ± Standard Deviation
Aethalometer (Magee Scientific AE33)	This Work (Butler et al.) El Asmar et al. (2024)	370, 470, 520, 590, 660, 880, 950	—	2.55 ± 0.43
Photoacoustic spectrometer (Droplet Technologies PAX)	Selimovic et al. (2018) Zeng et al. (2022)	401, 870	370, 880	2.97 ± 0.54
Continuous light absorption photometer	Marsavin et al. (2023)	467, 652	470, 660	2.82 ± 0.59
Satellite (AERONET)	Cazorla et al. (2013) Feng et al. (2013) Wang et al. (2016) Bian et al. (2020)	440, 870	470, 880	2.15 ± 0.37

392

393   The 1-minute average AAE for the three wavelength pairs are listed in the rightmost

394   column of Table 2. The 370, 880 and 470, 660 wavelength pairs have a 16% and 11% greater

395   value than the seven-wavelength power law fit in this work, whereas the 470, 880 wavelength

396   pair a 16% lesser value. These differences in average AAE indicate the uncertainty in interstudy

397   comparison is approximately $\pm$ 15%. Distributions of the coefficient of determination (r^2) for

398   each approach are also presented in Figure S11. A power law fit of 1-minute average data at all

399   seven wavelengths ($AAE_{7\lambda}$) yielded the highest average coefficient of determination ($r^2 = 0.88$),

400   followed closely by fitting data at only 370 and 880 nm ($r^2 = 0.87$). The lower average r^2 values

401   for power law fitting of data at 470 and 660 nm ($r^2 = 0.71$) and 470 and 880 nm ($r^2 = 0.60$)

402   suggest that the AAE values determined from these approaches are not as certain.

403

404   **4 Conclusion**

405   Fuel-based BC and BrC emission factors were calculated by the carbon balance method

406   with semi-continuous monitoring of a BC, CO, and CO_2 on ground and aerial platforms for four

407   days of prescribed burns. Aerial platform BC emission factors were measured under both flaming

408   and smoldering combustion, whereas ground platform BC and BrC emission factors skewed

409   towards almost entirely under smoldering combustion conditions. AAE, an aerosol optical

410   property, was similarly quantified for smoldering combustion. BC emission factors were found to

411   be poorly represented by a linear regression model based on MCE and were 2 times higher under

412   flaming combustion than smoldering combustion. In addition, BC emission factors may be used

413   in smoke models to improve wildland fire emissions inventories. BrC emission factors, estimated

414   using a BrC-specific absorption cross-section, were nearly 14 times greater than smoldering BC

415   emission factors and 7 times greater flaming BC emission factors. The study-average AAEs

416   indicated significant BrC absorption, especially in the near-UV spectrum, indicating that BrC is a

417   significant contributor to biomass smoke absorption of solar radiation. A fraction of this BrC

418   absorption may be attributable to so-called tar balls, which may comprise 5–30% of total $PM_{2.5}$

419   in wildfire smoke in the western United States (Adachi et al., 2024; Chakrabarty et al., 2023).

420   In future work, deployment of a multiwavelength aethalometer on the aerial platform,

421   would allow for Delta-C and AAE analyses to estimate BrC emission factors and optical

422   properties under flaming combustion. Multiwavelength aerosol absorption measurements on an

423   aerial platform across a wide range of combustion conditions would yield more representative

424   BrC emission factors and AAE values, which would inform how to model BrC emissions during

425   different combustion phases in fuel consumption models. Studies that quantify health impacts of

426   prescribed burn smoke with a chemical transport model will benefit from fuel-based emission

427   factors in this work and could determine the exposure concentrations of BC and BrC in $PM_{2.5}$.

428   The overall radiative effects of BC and BrC remains uncertain due to large uncertainties in global

429   emissions inventories from wildland fires sources (Bond et al., 2013). Further improvements in

430   bottom-up carbonaceous aerosol emissions inventories would constrain satellite retrievals of

431   aerosol optical depth used to model aerosol scattering and absorption in global climate models.

432   Further partnership between government agencies, private land owners, and tribal

433   nations will likely increase the frequency of prescribed burns, and thus possible health effects on

434   downwind communities (Miller et al., 2020). Continued field measurements of emission factors

435   with state-of-the-science platforms should focus on characterizing emission factors and optical

436   properties for ecosystems commonly burned in the western United States, like the mixed-conifer

437   forests studied here, Ponderosa pine forests, coastal forests, chaparral shrublands, and oak

438   savannas. Carbonaceous aerosol emission factors for each of these ecosystems remain

439   understudied, especially for BrC, and likely vary across ecosystems depending on fuel moisture

440   content, fuel types, and combustion efficiency of burn. In parallel, future studies could also

441   investigate the toxicity of BC and BrC emitted by prescribed burns, which may vary depending

442   on combustion conditions and fuels burned.

443

444   **Author Contribution**

445   **James D.A. Butler:** Conceptualization, Data Curation, Formal Analysis, Investigation,

446   Methodology, Resources, Visualization, Writing – original draft, Writing – review and editing.

447   **Afsara Tasnia:** Data Curation, Investigation, Methodology, Resources, Writing – review and

448   editing.

449   **Deep Sengupta:** Data Curation, Investigation, Methodology, Resources.

450   **Nathan Kreisberg:** Data Curation, Investigation, Methodology, Resources, Writing – review

451   and editing.

452 **Kelley C. Barsanti:** Conceptualization, Funding Acquisition, Methodology, Project

453 Administration, Supervision, Writing – review and editing.

454 **Allen H Goldstein:** Conceptualization, Funding Acquisition, Methodology, Project

455 Administration, Supervision, Writing – review and editing.

456 **Chelsea V. Preble:** Conceptualization, Methodology, Resources, Writing – review and editing.

457 **Rebecca A. Sugrue:** Resources, Writing – review and editing.

458 **Thomas W. Kirchstetter:** Conceptualization, Funding Acquisition, Methodology, Writing –

459 original draft, Writing – review and editing.

460

Competing interests

462 We declare that co-author Barsanti is on the editorial board of the journal *Atmospheric Chemistry*

463 *and Physics.*

464

Code/Data Availability

466 Data and code available upon request.

467

Acknowledgement

469   This work was supported by the California Air Resources Board (CARB) under contract

470 19RD008 and the California Department of Forestry and Fire Protection (CAL FIRE). Butler,

471 Kirchstetter, Preble, and Sugrue also acknowledge support of the Department of Energy under

472 Contract No. DEAC02-05CH11231. The statements and conclusions herein are those of the

473 authors and do not necessarily reflect the views of the project sponsors. We thank Ariel

474 Roughton, Rob York, John Battles, Scott Stephens and the staff of the Blodgett Forest Research

475 Station for their work to conduct the prescribed burns, feed and house the research team, and

476 ensure safety when taking field measurements; Coty Jen for her feedback on early analyses;

477 Drew Hill for his assistance on the Delta-C methodology; Adam Wise for development of the

478 photographs in Key Figure, Figure S2, and Figure S9; and Robert Harley for his review of early

479 drafts.

480

References

Adachi, K., Dibb, J. E., Katich, J. M., Schwarz, J. P., Guo, H., Campuzano-Jost, P., Jimenez, J. L., Peischl, J., Holmes, C. D., and Crawford, J.: Occurrence, abundance, and formation of atmospheric tarballs from a wide range of wildfires in the western US, Atmospheric Chemistry and Physics, 24, 10985–11004, https://doi.org/10.5194/acp-24-10985-2024, 2024.

Aerosol d.o.o.: Aethalometer(R) - AE36s: Expand the fronteirs of aerosol Science with cutting-edge Black Carbon instrument, Aerosol Magee Scientific, Ljubljana, Slovenia, 2024.

Akagi, S. K., Yokelson, R. J., Wiedinmyer, C., Alvarado, M. J., Reid, J. S., Karl, T., Crounse, J. D., and Wennberg, P. O.: Emission factors for open and domestic biomass burning for use in atmospheric models, Atmospheric Chemistry and Physics, 11, 4039–4072, https://doi.org/10.5194/acp-11-4039-2011, 2011.

Andreae, M. O.: Emission of trace gases and aerosols from biomass burning – an updated assessment, Atmospheric Chemistry and Physics, 19, 8523–8546, https://doi.org/10.5194/acp-19-8523-2019, 2019.

Aurell, J. and Gullett, B. K.: Emission Factors from Aerial and Ground Measurements of Field and Laboratory Forest Burns in the Southeastern U.S.: PM2.5, Black and Brown Carbon, VOC, and PCDD/PCDF, Environ. Sci. Technol., 47, 8443–8452, https://doi.org/10.1021/es402101k, 2013.

Aurell, J., Gullett, B., Holder, A., Kiros, F., Mitchell, W., Watts, A., and Ottmar, R.: Wildland fire emission sampling at Fishlake National Forest, Utah using an unmanned aircraft system, Atmospheric Environment, 247, 118193, https://doi.org/10.1016/j.atmosenv.2021.118193, 2021.

Bian, Q., Ford, B., Pierce, J. R., and Kreidenweis, S. M.: A Decadal Climatology of Chemical, Physical, and Optical Properties of Ambient Smoke in the Western and Southeastern United States, Journal of Geophysical Research: Atmospheres, 125, e2019JD031372, https://doi.org/10.1029/2019JD031372, 2020.

Binte Shahid, S., Lacey, F. G., Wiedinmyer, C., Yokelson, R. J., and Barsanti, K. C.: NEIVAv1.0: Next-generation Emissions InVentory expansion of Akagi et al. (2011) version 1.0, Geoscientific Model Development, 17, 7679–7711, https://doi.org/10.5194/gmd-17-7679-2024, 2024.

Bond, T. C., Streets, D. G., Yarber, K. F., Nelson, S. M., Woo, J.-H., and Klimont, Z.: A technology-based global inventory of black and organic carbon emissions from combustion, Journal of Geophysical Research: Atmospheres, 109, https://doi.org/10.1029/2003JD003697, 2004.

Bond, T. C., Doherty, S. J., Fahey, D. W., Forster, P. M., Berntsen, T., DeAngelo, B. J., Flanner, M. G., Ghan, S., Kärcher, B., Koch, D., Kinne, S., Kondo, Y., Quinn, P. K., Sarofim, M. C., Schultz, M. G., Schulz, M., Venkataraman, C., Zhang, H., Zhang, S., Bellouin, N., Guttikunda, S. K., Hopke, P. K., Jacobson, M. Z., Kaiser, J. W., Klimont, Z., Lohmann, U., Schwarz, J. P., Shindell, D., Storelvmo, T., Warren, S. G., and Zender, C. S.: Bounding the role of black carbon

in the climate system: A scientific assessment, Journal of Geophysical Research: Atmospheres, 118, 5380–5552, https://doi.org/10.1002/jgrd.50171, 2013.

Burling, I. R., Yokelson, R. J., Akagi, S. K., Urbanski, S. P., Wold, C. E., Griffith, D. W. T., Johnson, T. J., Reardon, J., and Weise, D. R.: Airborne and ground-based measurements of the trace gases and particles emitted by prescribed fires in the United States, Atmospheric Chemistry and Physics, 11, 12197–12216, https://doi.org/10.5194/acp-11-12197-2011, 2011.

California Air Resources Board: California's Black Carbon Emission Inventory–Technical Support Document, 2016.

California Air Resources Board: Greenhouse Gas Emissions of Contemporary Wildfire, Prescribed Fire, and Forest Management Activities, California Air Resources Board, Sacramento, CA, 2020.

Caubel, J. J., Cados, T. E., and Kirchstetter, T. W.: A new black carbon sensor for dense air quality monitoring networks, Sensors, 18, 738, https://doi.org/10.3390/s18030738, 2018.

Cazorla, A., Bahadur, R., Suski, K. J., Cahill, J. F., Chand, D., Schmid, B., Ramanathan, V., and Prather, K. A.: Relating aerosol absorption due to soot, organic carbon, and dust to emission sources determined from in-situ chemical measurements, Atmospheric Chemistry and Physics, 13, 9337–9350, https://doi.org/10.5194/acp-13-9337-2013, 2013.

Chakrabarty, R. K., Shetty, N. J., Thind, A. S., Beeler, P., Sumlin, B. J., Zhang, C., Liu, P., Idrobo, J. C., Adachi, K., Wagner, N. L., Schwarz, J. P., Ahern, A., Sedlacek, A. J., Lambe, A., Daube, C., Lyu, M., Liu, C., Herndon, S., Onasch, T. B., and Mishra, R.: Shortwave absorption by wildfire smoke dominated by dark brown carbon, Nat. Geosci., 16, 683–688, https://doi.org/10.1038/s41561-023-01237-9, 2023.

Chelluboyina, G. S., Kapoor, T. S., and Chakrabarty, R. K.: Dark brown carbon from wildfires: a potent snow radiative forcing agent?, npj Clim Atmos Sci, 7, 1–10, https://doi.org/10.1038/s41612-024-00738-7, 2024.

Chen, L.-W. A., Moosmüller, H., Arnott, W. P., Chow, J. C., Watson, J. G., Susott, R. A., Babbitt, R. E., Wold, C. E., Lincoln, E. N., and Hao, W. M.: Emissions from Laboratory Combustion of Wildland Fuels: Emission Factors and Source Profiles, Environ. Sci. Technol., 41, 4317–4325, https://doi.org/10.1021/es062364i, 2007.

Chow, J. C., Watson, J. G., Lowenthal, D. H., Antony Chen, L.-W., and Motallebi, N.: PM2.5 source profiles for black and organic carbon emission inventories, Atmospheric Environment, 45, 5407–5414, https://doi.org/10.1016/j.atmosenv.2011.07.011, 2011.

Connolly, R., Marlier, M. E., Garcia-Gonzales, D. A., Wilkins, J., Su, J., Bekker, C., Jung, J., Bonilla, E., Burnett, R. T., Zhu, Y., and Jerrett, M.: Mortality attributable to PM2.5 from wildland fires in California from 2008 to 2018, Science Advances, 10, eadl1252, https://doi.org/10.1126/sciadv.adl1252, 2024.

Cruz Núñez, X., Villers Ruiz, L., and Gay García, C.: Black carbon and organic carbon emissions from wildfires in Mexico, Atmósfera, 27, 165–172, https://doi.org/10.1016/S0187-6236(14)71107-5, 2014.

Dong, Q., Meng, X., Gong, J., and Zhu, T.: A review of advances in black carbon exposure assessment and health effects, CSB, 69, 703–716, https://doi.org/10.1360/TB-2023-0409, 2023.

El Asmar, R., Li, Z., Tanner, D. J., Hu, Y., O'Neill, S., Huey, L. G., Odman, M. T., and Weber, R. J.: A multi-site passive approach to studying the emissions and evolution of smoke from prescribed fires, Atmospheric Chemistry and Physics, 24, 12749–12773, https://doi.org/10.5194/acp-24-12749-2024, 2024.

Feng, Y., Ramanathan, V., and Kotamarthi, V. R.: Brown carbon: a significant atmospheric absorber of solar radiation?, Atmospheric Chemistry and Physics, 13, 8607–8621, https://doi.org/10.5194/acp-13-8607-2013, 2013.

Grahame, T. J., Klemm, R., and Schlesinger, R. B.: Public health and components of particulate matter: The changing assessment of black carbon, Journal of the Air & Waste Management Association, 64, 620–660, https://doi.org/10.1080/10962247.2014.912692, 2014.

Hadley, O. L. and Kirchstetter, T. W.: Black-carbon reduction of snow albedo, Nature Clim Change, 2, 437–440, https://doi.org/10.1038/nclimate1433, 2012.

Harrison, R. M., Beddows, D. C. S., Jones, A. M., Calvo, A., Alves, C., and Pio, C.: An evaluation of some issues regarding the use of aethalometers to measure woodsmoke concentrations, Atmospheric Environment, 80, 540–548, https://doi.org/10.1016/j.atmosenv.2013.08.026, 2013.

Hosseini, S., Urbanski, S. P., Dixit, P., Qi, L., Burling, I. R., Yokelson, R. J., Johnson, T. J., Shrivastava, M., Jung, H. S., Weise, D. R., Miller, J. W., and Cocker III, D. R.: Laboratory characterization of PM emissions from combustion of wildland biomass fuels, Journal of Geophysical Research: Atmospheres, 118, 9914–9929, https://doi.org/10.1002/jgrd.50481, 2013.

Huang, J., Hopke, P. K., Choi, H.-D., Laing, J. R., Cui, H., Zananski, T. J., Chandrasekaran, S. R., Rattigan, O. V., and Holsen, T. M.: Mercury (Hg) emissions from domestic biomass combustion for space heating, Chemosphere, 84, 1694–1699, https://doi.org/10.1016/j.chemosphere.2011.04.078, 2011.

Ivančič, M., Gregorič, A., Lavrič, G., Alföldy, B., Ježek, I., Hasheminassab, S., Pakbin, P., Ahangar, F., Sowlat, M., Boddeker, S., and Rigler, M.: Two-year-long high-time-resolution apportionment of primary and secondary carbonaceous aerosols in the Los Angeles Basin using an advanced total carbon–black carbon (TC-BC(λ)) method, Science of The Total Environment, 848, 157606, https://doi.org/10.1016/j.scitotenv.2022.157606, 2022.

Janssen, N. A. H., Hoek, G., Simic-Lawson, M., Fischer, P., van Bree, L., ten Brink, H., Keuken, M., Atkinson, R. W., Anderson, H. R., Brunekreef, B., and Cassee, F. R.: Black carbon as an

590 additional indicator of the adverse health effects of airborne particles compared with PM10 and
591 PM2.5, Environ Health Perspect, 119, 1691–1699, https://doi.org/10.1289/ehp.1003369, 2011.

592 Kaspari, S., McKenzie Skiles, S., Delaney, I., Dixon, D., and Painter, T. H.: Accelerated glacier
593 melt on Snow Dome, Mount Olympus, Washington, USA, due to deposition of black carbon and
594 mineral dust from wildfire, Journal of Geophysical Research: Atmospheres, 120, 2793–2807,
595 https://doi.org/10.1002/2014JD022676, 2015.

596 Keane, R. E. and Lutes, D.: First-Order Fire Effects Model (FOFEM), in: Encyclopedia of
597 Wildfires and Wildland-Urban Interface (WUI) Fires, edited by: Manzello, S. L., Springer
598 International Publishing, Cham, 1–5, https://doi.org/10.1007/978-3-319-51727-8_74-1, 2018.

599 Kirchstetter, T. W. and Thatcher, T. L.: Contribution of organic carbon to wood smoke particulate
600 matter absorption of solar radiation, Atmospheric Chemistry and Physics, 12, 6067–6072,
601 https://doi.org/10.5194/acp-12-6067-2012, 2012.

602 Kirchstetter, T. W., Novakov, T., and Hobbs, P. V.: Evidence that the spectral dependence of light
603 absorption by aerosols is affected by organic carbon, Journal of Geophysical Research:
604 Atmospheres, 109, https://doi.org/10.1029/2004JD004999, 2004.

605 Larkin, N. K., Raffuse, S. M., Huang, S., Pavlovic, N., Lahm, P., and Rao, V.: The
606 Comprehensive Fire Information Reconciled Emissions (CFIRE) inventory: Wildland fire
607 emissions developed for the 2011 and 2014 U.S. National Emissions Inventory, Journal of the
608 Air & Waste Management Association, 70, 1165–1185,
609 https://doi.org/10.1080/10962247.2020.1802365, 2020.

610 BlueSky Modeling Framework: https://www.airfire.org/data/bluesky, last access: 12 November
611 2024.

612 Laskin, A., Laskin, J., and Nizkorodov, S. A.: Chemistry of Atmospheric Brown Carbon, Chem.
613 Rev., 115, 4335–4382, https://doi.org/10.1021/cr5006167, 2015.

614 Levinson, R., Akbari, H., and Berdahl, P.: Measuring solar reflectance—Part I: Defining a metric
615 that accurately predicts solar heat gain, Solar Energy, 84, 1717–1744,
616 https://doi.org/10.1016/j.solener.2010.04.018, 2010.

617 Li, J. and Li, Y.: Ozone deterioration over North China plain caused by light absorption of black
618 carbon and organic carbon, Atmospheric Environment, 313, 120048,
619 https://doi.org/10.1016/j.atmosenv.2023.120048, 2023.

620 Liu, C., Chung, C. E., Yin, Y., and Schnaiter, M.: The absorption Ångström exponent of black
621 carbon: from numerical aspects, Atmospheric Chemistry and Physics, 18, 6259–6273,
622 https://doi.org/10.5194/acp-18-6259-2018, 2018.

623 Lutes, D. C.: FOFEM 6.7 User Guide, United States Forest Service, 2020.

Maji, K. J., Li, Z., Vaidyanathan, A., Hu, Y., Stowell, J. D., Milando, C., Wellenius, G., Kinney, P. L., Russell, A. G., and Odman, M. T.: Estimated Impacts of Prescribed Fires on Air Quality and Premature Deaths in Georgia and Surrounding Areas in the US, 2015–2020, Environ. Sci. Technol., https://doi.org/10.1021/acs.est.4c00890, 2024.

Marsavin, A., Gageldonk, R. van, Bernays, N., May, N. W., Jaffe, D. A., and Fry, J. L.: Optical properties of biomass burning aerosol during the 2021 Oregon fire season: comparison between wild and prescribed fires, Environ. Sci.: Atmos., 3, 608–626, https://doi.org/10.1039/D2EA00118G, 2023.

May, A. A., McMeeking, G. R., Lee, T., Taylor, J. W., Craven, J. S., Burling, I., Sullivan, A. P., Akagi, S., Collett, J. L., Flynn, M., Coe, H., Urbanski, S. P., Seinfeld, J. H., Yokelson, R. J., and Kreidenweis, S. M.: Aerosol emissions from prescribed fires in the United States: A synthesis of laboratory and aircraft measurements, Journal of Geophysical Research: Atmospheres, 119, 11,826-11,849, https://doi.org/10.1002/2014JD021848, 2014.

McMeeking, G. R., Kreidenweis, S. M., Baker, S., Carrico, C. M., Chow, J. C., Collett, J. L., Hao, W. M., Holden, A. S., Kirchstetter, T. W., Malm, W. C., Moosmüller, H., Sullivan, A. P., and Wold, C. E.: Emissions of trace gases and aerosols during the open combustion of biomass in the laboratory, Journal of Geophysical Research: Atmospheres, 114, https://doi.org/10.1029/2009JD011836, 2009.

Miller, R. K., Field, C. B., and Mach, K. J.: Barriers and enablers for prescribed burns for wildfire management in California, Nat Sustain, 3, 101–109, https://doi.org/10.1038/s41893-019-0451-7, 2020.

Mok, J., Krotkov, N. A., Arola, A., Torres, O., Jethva, H., Andrade, M., Labow, G., Eck, T. F., Li, Z., Dickerson, R. R., Stenchikov, G. L., Osipov, S., and Ren, X.: Impacts of brown carbon from biomass burning on surface UV and ozone photochemistry in the Amazon Basin, Sci Rep, 6, 36940, https://doi.org/10.1038/srep36940, 2016.

Nelson Jr., R. M.: An evaluation of the carbon balance technique for estimating emission factors and fuel consumption in forest fires, Res. Pap. SE-231. Asheville, NC: U.S. Department of Agriculture, Forest Service, Southeastern Forest Experiment Station, 231, 9, https://doi.org/10.2737/SE-RP-231, 1982.

North, M., Collins, B., Safford, H., and Stephenson, N.: Montane Forests, in: Ecosystems of California, University of California Press, 553–578, 2016.

Ottmar, R. D.: Wildland fire emissions, carbon, and climate: Modeling fuel consumption, Forest Ecology and Management, 317, 41–50, https://doi.org/10.1016/j.foreco.2013.06.010, 2014.

Selimovic, V., Yokelson, R. J., Warneke, C., Roberts, J. M., de Gouw, J., Reardon, J., and Griffith, D. W. T.: Aerosol optical properties and trace gas emissions by PAX and OP-FTIR for laboratory-simulated western US wildfires during FIREX, Atmospheric Chemistry and Physics, 18, 2929–2948, https://doi.org/10.5194/acp-18-2929-2018, 2018.

Stampfer, O., Austin, E., Ganuelas, T., Fiander, T., Seto, E., and Karr, C. J.: Use of low-cost PM monitors and a multi-wavelength aethalometer to characterize PM2.5 in the Yakama Nation reservation, Atmospheric Environment, 224, 117292, https://doi.org/10.1016/j.atmosenv.2020.117292, 2020.

Steel, Z. L., Foster, D., Coppoletta, M., Lydersen, J. M., Stephens, S. L., Paudel, A., Markwith, S. H., Merriam, K., and Collins, B. M.: Ecological resilience and vegetation transition in the face of two successive large wildfires, Journal of Ecology, 109, 3340–3355, https://doi.org/10.1111/1365-2745.13764, 2021.

Sugrue, R. A., Preble, C. V., Butler, J. D. A., Redon-Gabel, A. J., Marconi, P., Shetty, K. D., Hill, L. A. L., Amezcua-Smith, A. M., Lukanov, B. R., and Kirchstetter, T. W.: The value of adding black carbon to community monitoring of particulate matter, Atmospheric Environment, 325, 120434, https://doi.org/10.1016/j.atmosenv.2024.120434, 2024.

Tasnia, A., Lara, G., Foster, D., Sengupta, D., Butler, J. D. A., Kirchstetter, T. W., York, R., Kreisberg, N. M., Goldstein, A. H., Battles, J. J., and Barsanti, K. C.: Comprehensive Fuel and Emissions Measurements Highlight Uncertainties in Smoke Production Using Predictive Modeling Tools, ACS EST Air, 2, 982–997, https://doi.org/10.1021/acsestair.4c00142, 2025.

Thomas, S. C. and Martin, A. R.: Carbon Content of Tree Tissues: A Synthesis, Forests, 3, 332–352, https://doi.org/10.3390/f3020332, 2012.

Urbanski, S.: Wildland fire emissions, carbon, and climate: Emission factors, Forest Ecology and Management, 317, 51–60, https://doi.org/10.1016/j.foreco.2013.05.045, 2014.

Urbanski, S. P., Hao, W. M., and Baker, S.: Chapter 4 Chemical Composition of Wildland Fire Emissions, in: Developments in Environmental Science, vol. 8, edited by: Bytnerowicz, A., Arbaugh, M. J., Riebau, A. R., and Andersen, C., Elsevier, 79–107, https://doi.org/10.1016/S1474-8177(08)00004-1, 2008.

US Environmental Protection Agency: 2020 National Emissions Inventory Technical Support Document: Fires –Wild, Prescribed, and Agricultural Field Burning, US Environmental Protection Agency, Research Triangle Park, NC, 2023.

SPECIATE: https://www.epa.gov/air-emissions-modeling/speciate-0, last access: 16 January 2025.

Wagstaff, M., Henderson, S. B., McLean, K. E., and Brauer, M.: Development of methods for citizen scientist mapping of residential woodsmoke in small communities, Journal of Environmental Management, 311, 114788, https://doi.org/10.1016/j.jenvman.2022.114788, 2022.

Wang, X., Heald, C. L., Sedlacek, A. J., de Sá, S. S., Martin, S. T., Alexander, M. L., Watson, T. B., Aiken, A. C., Springston, S. R., and Artaxo, P.: Deriving brown carbon from multiwavelength absorption measurements: method and application to AERONET and Aethalometer observations,

696 Atmospheric Chemistry and Physics, 16, 12733–12752, https://doi.org/10.5194/acp-16-12733-
697 2016, 2016.

698 Wang, Y., Huang, J., Zananski, T. J., Hopke, P. K., and Holsen, T. M.: Impacts of the Canadian
699 Forest Fires on Atmospheric Mercury and Carbonaceous Particles in Northern New York,
700 Environ. Sci. Technol., 44, 8435–8440, https://doi.org/10.1021/es1024806, 2010.

701 Wang, Y., Hopke, P. K., Rattigan, O. V., Xia, X., Chalupa, D. C., and Utell, M. J.:
702 Characterization of Residential Wood Combustion Particles Using the Two-Wavelength
703 Aethalometer, Environ. Sci. Technol., 45, 7387–7393, https://doi.org/10.1021/es2013984, 2011a.

704 Wang, Y., Hopke, P. K., and Utell, M. J.: Urban-scale Spatial-temporal Variability of Black
705 Carbon and Winter Residential Wood Combustion Particles, Aerosol Air Qual. Res., 11, 473–
706 481, https://doi.org/10.4209/aaqr.2011.01.0005, 2011b.

707 Ward, D. E. and Radke, L. F.: Emissions Measurements from Vegetation Fires: A Comparative
708 Evaluation of Methods and Results, in: Fire in the Environmentl: The Ecological, Atmospheric,
709 and Climatic Importance of Vegetation Fires, John Wiley & Sons Ltd., 53–76, 1993.

710 Wiedinmyer, C., Quayle, B., Geron, C., Belote, A., McKenzie, D., Zhang, X., O'Neill, S., and
711 Wynne, K. K.: Estimating emissions from fires in North America for air quality modeling,
712 Atmospheric Environment, 40, 3419–3432, https://doi.org/10.1016/j.atmosenv.2006.02.010,
713 2006.

714 Wu, X., Sverdrup, E., Mastrandrea, M. D., Wara, M. W., and Wager, S.: Low-intensity fires
715 mitigate the risk of high-intensity wildfires in California's forests, Science Advances, 9,
716 eadi4123, https://doi.org/10.1126/sciadv.adi4123, 2023.

717 Yang, S., Xu, B., Cao, J., Zender, C. S., and Wang, M.: Climate effect of black carbon aerosol in
718 a Tibetan Plateau glacier, Atmospheric Environment, 111, 71–78,
719 https://doi.org/10.1016/j.atmosenv.2015.03.016, 2015.

720 Yokelson, R. J., Burling, I. R., Gilman, J. B., Warneke, C., Stockwell, C. E., de Gouw, J., Akagi,
721 S. K., Urbanski, S. P., Veres, P., Roberts, J. M., Kuster, W. C., Reardon, J., Griffith, D. W. T.,
722 Johnson, T. J., Hosseini, S., Miller, J. W., Cocker III, D. R., Jung, H., and Weise, D. R.: Coupling
723 field and laboratory measurements to estimate the emission factors of identified and unidentified
724 trace gases for prescribed fires, Atmospheric Chemistry and Physics, 13, 89–116,
725 https://doi.org/10.5194/acp-13-89-2013, 2013.

726 Zeng, L., Dibb, J., Scheuer, E., Katich, J. M., Schwarz, J. P., Bourgeois, I., Peischl, J., Ryerson,
727 T., Warneke, C., Perring, A. E., Diskin, G. S., DiGangi, J. P., Nowak, J. B., Moore, R. H.,
728 Wiggins, E. B., Pagonis, D., Guo, H., Campuzano-Jost, P., Jimenez, J. L., Xu, L., and Weber, R.
729 J.: Characteristics and evolution of brown carbon in western United States wildfires,
730 Atmospheric Chemistry and Physics, 22, 8009–8036, https://doi.org/10.5194/acp-22-8009-2022,
731 2022.

732   Zhang, A., Wang, Y., Zhang, Y., Weber, R. J., Song, Y., Ke, Z., and Zou, Y.: Modeling the global
733   radiative effect of brown carbon: a potentially larger heating source in the tropical free
734   troposphere than black carbon, Atmospheric Chemistry and Physics, 20, 1901–1920,
735   https://doi.org/10.5194/acp-20-1901-2020, 2020.

736